A METHOD FOR DISPERSING PARTICLE FILLERS IN THERMOPLASTIC COMPOSITES USING COMMINGLED YARNS

Joanna C. H. Wong[1,2], Nadine Hertaeg[1] and Paolo Ermanni[1]

[1] ETH Zurich, Laboratory of Composite Materials and Adaptive Structures, Leonhardstrasse 21, 8092 Zurich, Switzerland, www.structures.ethz.ch

[2] Department of Mechanical and Manufacturing Engineering, University of Calgary, 2500 University Drive NW, Calgary, Alberta, Canada, T2N 1N4, wong.j@ucalgary.ca

Keywords: Thermoplastic composites, Particle-toughening, Commingled yarns, Processing, Dispersions

ABSTRACT

The incorporation of particles in a polymer material has the potential to increase the toughness of the polymer, and thereby potentially also the toughness of a fibre-reinforced composite material in which the polymer is used as a matrix. Particle-toughening of thermoset polymers is an established state-of-the art technique; the toughness of thermoplastic polymers – already higher than that of thermosets – may be further enhanced by using the same particle-toughening principle, leading to materials with even better performance. We present a simple and effective method for dispersing alumina nanoparticles inside a non-consolidated woven textile of continuous glass fibre-polyamide 6 commingled yarns that, when consolidated, produce thermoplastic composites with particle-filled matrices. The wet pick up of the particle suspension by the textile and the dispersion quality of the particles inside the fibrous architecture is reported. The effect of the hard Al_2O_3 particles on the fracture properties of the PA6 polymer is studied using single-edge cracked plate tests, indicating increased J_{Ic} values due to the particles in the PA6 matrix system. However, double cantilever beam tests investigating the effect of the particles on the interlaminar fracture toughness of the fibre-reinforced thermoplastic composite material were inconclusive due to the failure of the material by transverse yarn debonding rather than by interlaminar failure.

1 INTRODUCTION

In polymer materials, hard inorganic particle fillers have been reported to operate as toughening agents by dissipating energy through mechanisms such as de-bonding, particle fracture, and crack deflection.[1-3] The effects of particle-toughening have been observed in both brittle thermosetting polymers, e.g. epoxy, as well as in comparatively tougher thermoplastic polymers, e.g. polyamide.[4-6] For example, Figure 1 shows the ability of alumina particles to deflect cracks and promote shear band formation in polyamide 6 (PA6), a relatively tough polymer. In fibre-reinforced polymer composites, higher toughness properties in the polymer matrix material are correlated positively to higher fracture toughness in the composite material.[7-9] In the last decades, numerous investigations have presented various strategies to toughen epoxy systems with particles.[1-3,6-10] However, investigations into the effects of particle-toughening on thermoplastic composites are scarcer, as the process is hampered by difficulties in dispersing the particles in the high viscosity thermoplastic polymer melts.

This paper describes an original and simple method that was used to manufacture particle-toughened fibre-reinforced thermoplastic composites. This approach involves dispersing ceramic particles into a fabric made of commingled yarns by means of an aqueous suspension, and takes advantage of the zeta potential of the colloidal particles to disperse the particles in water. This process has already been used to disperse alumina particles for foaming applications.[11-14] The aqueous colloidal suspension infiltrates the unoccupied spaces within the commingled yarn textile, dispersing particles into the free space between the fibres. When the water phase is removed from the commingled yarn fabric by evaporation, the ceramic particles remain in the fabric and may act as

toughening agents in the thermoplastic matrix once the commingled yarn fabric is consolidated under heat and pressure.

The purpose of this paper is to investigate the effects of adding ceramic nanoparticles to a fibre-reinforced thermoplastic composite system via the presented suspension method. The effects of compounding the nanoparticles into the neat polymer system are studied for reference.

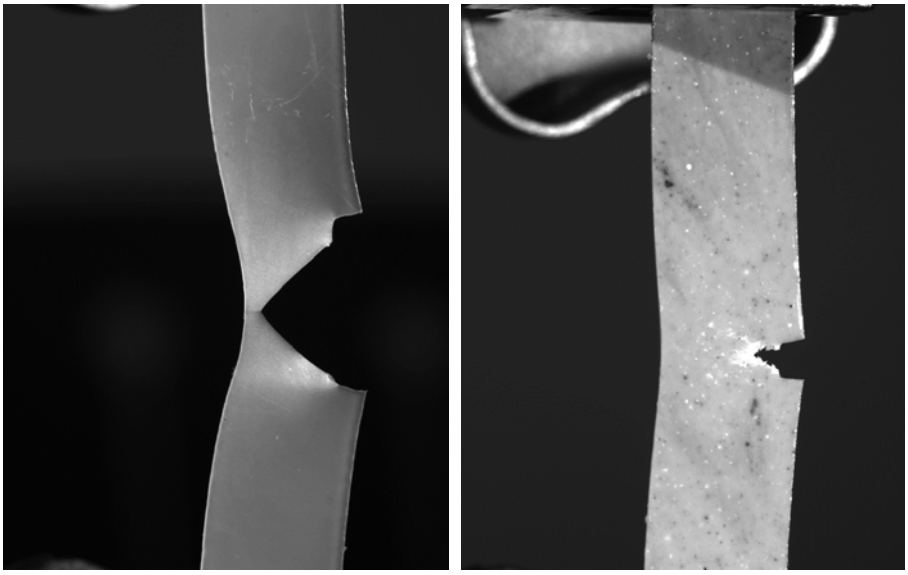

Figure 1: Single edge cracked plate specimens showing (left) sharp crack tip propagation in neat PA 6 material, and (right) shear band formation and crack tip deflection in compounded PA6 material containing 10 % v/v alumina particles.

2 EXPERIMENTAL DETAILS

2.1 Materials

An E-glass-fibre reinforced black-dyed polyamide 6 (PA6) (T_{melt} = 220 °C) commingled yarn 2/2 twill woven fabric (650 g/m^2, 480 tex) from Comfil (Denmark) was used as the thermoplastic composite intermediate material. The glass fibres and PA6 fibres were measured to have diameters of 14 μm and 36 μm, respectively, and the material was reported to have a fibre volume content of ~ 44%. For the non-fibre-reinforced polymer reference samples, PA6 pellets of the same polymer grade as that used in the commingled yarn were obtained from Comfil (Denmark). The ceramic nanoparticles used were alumina particles from Ceralox (USA) with an average diameter of 200 ± 100 nm and a point of zero charge at pH ≈ 10. Additional chemicals used included 1 M hydrochloric acid (HCl) (Titrisol®, Merck kGaA, Germany) and deionized water.

2.2 Material characterization

The commingled yarns were characterized by differential scanning calorimetry (DSC) (DSC 1, Mettler Toledo, Switzerland) and by thermogravimetric analysis (TGA) (Pyris 1, Perkin Elmer, Switzerland) to determine the melting temperature of the polymer and the fibre volume content of the commingled yarns, respectively. Imaging was performed by optical microscopy (DMRXA, Leica, Germany) and scanning electron microscopy (SEM) (LEO 1530 Gemini, Zeiss, Germany). Sample preparation for optical imaging involved embedding the samples in resin (SpeciFix 20, Struers, USA) and polishing (Abramin, Struers, Denmark) using successively fine grained discs (MD Piano 120 to MD Nap, Stuers, Denmark) and diamond suspensions (DiaPro Allegro/Largo 9 μm to Diapro Nap R 1 μm) to obtain clean cross-sections. Sample preparation for SEM involved coating the samples with a 3 nm thick layer of platinum using a sputter coater (CCU-010, Safematic, Switzerland).

2.3 Sample preparation of reference PA6/Al_2O_3 composites

Samples of PA6/Al_2O composites were prepared by compounding measured amounts of PA6 pellets and Al_2O_3 in a twin screw extruder (Plasti-corder, Brabender, Germany) at 240 °C and a mixing speed of 15 rpm for 15 min. The resulting compounded melt was removed from the twin screw extruder, cooled to room temperature, and then placed inside a vacuum oven at 60 °C overnight to avoid water absorption into the PA6. The extruded material was then moulded inside an aluminium mould between two layers of polyimide into a 0.5 mm thick flat plate using a press (Machine N° C3426, Rondol, France) at a temperature of 240 °C and an applied pressure of 50 kN over a platen area of 300 mm × 300 mm for 2 min, then cooled inside a different press machine (THB 400, Fontijne, Netherlands) which was water-cooled. Dog bone and single-edge cracked plate (SECP) specimens were stamped (S1 C95032.4, Wallace, England) out of the pressed plate.

2.4 Sample preparation of GF-PA6/Al_2O_3 composites

The GF-PA6/Al_2O_3 composites were prepared by soaking stacks of 16 layers (~20 mm in thickness when uncompressed) of 100 mm × 200 mm commingled yarn textiles in aqueous suspensions of Al_2O_3 with concentrations between 0 and 200 g/L. These suspensions were prepared by mixing measured weights of Al_2O_3 into a volume of water whose pH was adjusted to ~2 by adding HCl. The addition of the acid ensures that the Al_2O_3 particles have a high zeta potential which makes the suspensions stable against agglomeration. The suspensions were subjected to an ultrasonic bath (Elmasonic S 30 (H), Elma Schmidbauer GmbH, Germany) for 10 min at room temperature to break down large agglomerations. The commingled yarn textiles were placed inside a 135 mm × 200 mm × 30 mm rectangular dish and soaked in the aqueous Al_2O_3 suspensions for 1 h to allow diffusion of the particles into the free spaces inside the textile architecture. Excess suspension was drained out and its volume measured to estimate the amount of suspension picked up by the textiles. The wet stack of textiles were placed in a vacuum oven at 60 °C overnight.

The dried fabrics containing the particles were arranged in a mould, and a non-stick layer of Teflon was placed between the 8th and the 9th layers to form the pre-crack. The whole stack was consolidated into a 5 mm thick plate using a hot press (TP 400, Fontijne, Netherlands) in a compression moulding process at a temperature of 240 °C and a pressure of 50 kN over a platen area of 320 mm ×320 mm for 5 min. The plate was cut into four 25 mm × 190 mm double cantilever beam (DCB) specimens using a cut-off saw (Diadisc 5200, Mutronic GmbH, Germany) and polished to smoothen any rough edges. Sample dimensions and weights were measured for density estimations.

2.5 Mechanical Testing

All mechanical tests were performed on a universal testing machine (Z005, Zwick/Roell, Germany) with a 5 kN load cell.

Tensile tests were done on the dog-bone specimens at a crosshead speed of 2 mm/min to determine the elastic modulus (E). A digital image correlation setup and software (Version 8, Vic-Snap Image Acquistion, Correlated Solutions, USA) was used to measure the corresponding strain.

The fracture toughness of the PA6/Al_2O_3 samples was measured using SECP tests. The notches were cut into the samples using a diamond wire saw (3242, Well, Switzerland) without additional sharpening of the notch. The SECP fracture tests were performed under uniform tension using a cross head speed of 5 mm/min. J integral curves were calculated using the method presented in ref [4] and [15].

Attempts to investigate the interlaminar fracture toughness of the GF-PA6/Al_2O_3 composites were made using the DCB specimens produced from the particle-filled commingled yarn textiles. To monitor the crack propagation, one side of the DCB specimens was spray painted white (RAL Buntlack, Seidenmatt, Mood, Switzerland) and 1 mm spaced lines were toner-transferred to the painted edge. The tops and bottoms of the samples were cleaned with acetone, and then roughened by grinding with sandpaper. Piano hinges (25mm heavy-duty steel backflap) were then glued on to the surfaces using a structural epoxy (Scotchweld™ DP 460, 3M, USA).[16][17] Due to poor adhesion between the adhesive and the piano hinge and DCB specimen, the bonded joint was reinforced with an

in-house made Brandt hinge-like clamp made of steel that prevented adhesive failure at the epoxy interface (see Figure 2).[18] However, to accommodate the Brandt hinge-like clamp, the thickness of the pre-crack had to be enlarged by 2 mm using the cut-out saw (Diadisc 5200, Mutronic, Germany).[19] This modification was several millimetres removed from the pre-crack tip, and thus did not affect the original crack opening.

Images and videos of the mechanical tests were recorded using a digital camera (Prosilica GT, Allied Vision Technologies, Canada).

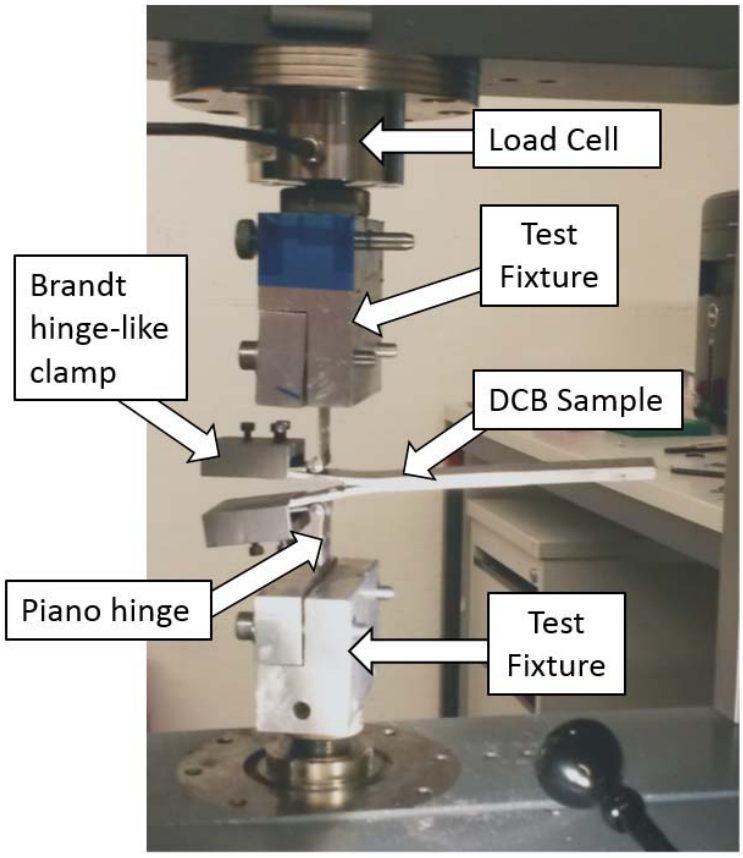

Figure 2: Photograph of DCB test set up showing Brandt hinge-like clamps used to secure piano hinges to the specimen.

3 RESULTS AND DISCUSSION

3.1 Deposition of particles into fabric via suspension method

Based on the excess volumes of suspension collected, the wet pick-up of the fabric stacks was between 300 and 350 mL of suspension, which corresponds to an uptake of 1.44 – 1.68 mL/g of fabric. The high uptake is attributed to both PA6's and glass' hydrophilicity and the capillary action between the individual fibres and between the fibre tows.

As the water evaporated, the particles were deposited onto the surfaces of the fibres. In low concentrations (<30 g/L), the particles deposited as a thin layer over the available surfaces with no noticeable preference for the GF or PA6 fibres. At higher concentrations, the particles were not able to maintain a stable dispersion as the water evaporated, resulting in the formation of large agglomerates distributed through the fibrous network. Figure 3 shows SEM images of the commingled yarns as they were received, and after of soaking the textiles in suspensions containing 24 and 121 g/L of Al_2O_3 nanoparticles. On the macroscale, the presence of the nanoparticles could be detected by eye as a thin whitish coating and/or grains of white agglomerates.

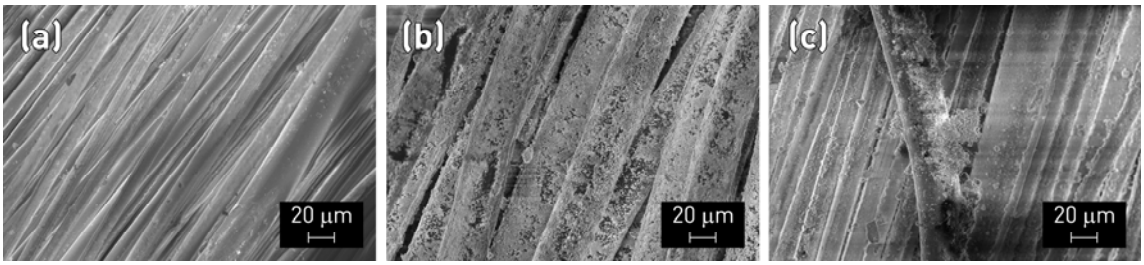

Figure 3: Scanning electron microscopy (SEM) images of commingled yarns as (a) received, and after soaking in Al_2O_3 dispersions with concentrations of (b) 24 g/L, and (c) 121 g/L. At lower concentrations, the nanoparticles tended to deposit evenly on to the surface of the fibres, while large agglomerates tended to form at higher concentrations.

Significant drainage and settling of the large agglomerates due to gravity was observed in the samples that were soaked in high concentration (>70 g/L) suspensions, resulting in a noticeable particle distribution gradient. In these cases, the bottom-most layers had disproportionately large amounts of particles. The effects of drainage may be minimized by processing the layers individually rather than as stack.

Because Al_2O_3 has a density of 3.95 g/cm^3, which is much higher than the densities of glass and PA6, which are reported as 2.4 g/cm^3 a and 1.12 g/cm^3 respectively, the addition of the Al_2O_3 particles to the GF-PA6 composite increased the overall densities of the composites. The amount of Al_2O_3 retained inside the final composite can be estimated by the difference in density between the particle-filled and non-particle-filled materials, assuming the absence of voids and a fixed fibre volume content value. Figure 4 shows the density of the Al_2O_3 particle-filled GF-PA6 composite and the corresponding theoretical Al_2O_3 volume content as a function of the concentration of Al_2O_3 in the suspension bath. These experimentally measured densities are expected to be lower than the theoretical densities due to the presence of voids and loss of fibrous material during processing. Loss of material and voids would explain the observation that the overall density appear to decrease in some samples. At the highest suspension concentration studied here, Al_2O_3 was calculated to represent almost 6% of the total composite volume, when the influence of voids was neglected.

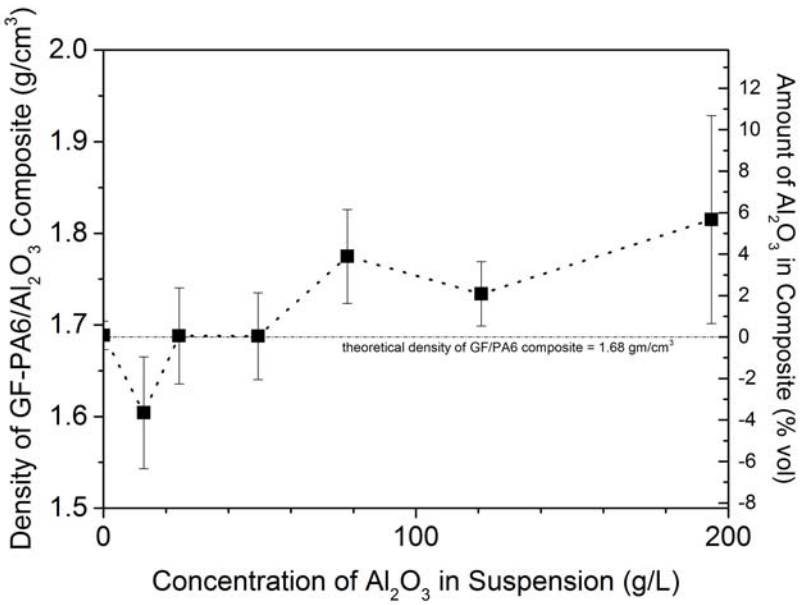

Figure 4: Density of GF-PA6/Al_2O_3 composites as a function of suspension bath concentration and the calculated volume fraction of Al_2O_3 in the final composite.

Optical microscopy analysis of the consolidated particle-filled commingled yarn textiles revealed the presence of large voids between fibre bundles and areas of dry fibre in all samples, indicating that the consolidation of the intermediate material should be improved by optimizing the processing conditions. The optical microscopy images in Figure 5 give representative examples of the cross-sections from GF-PA6/Al_2O_3 composite materials. The nanoparticles and agglomerates in the consolidated materials could not be resolved using the optical microscope. SEM imaging of the consolidated samples showed that the particles tended to be located near the fibres in agglomerations as shown in Figure 6. A closer examination of the particle-filled regions is provided in Figure 7, where the surface structure of the particle-rich areas was observed to differ from particle-poor regions. No investigations were done to determine if these differences are only cosmetic or if the particles affect the crystallinity of the polymer material with which they are in intimate contact.

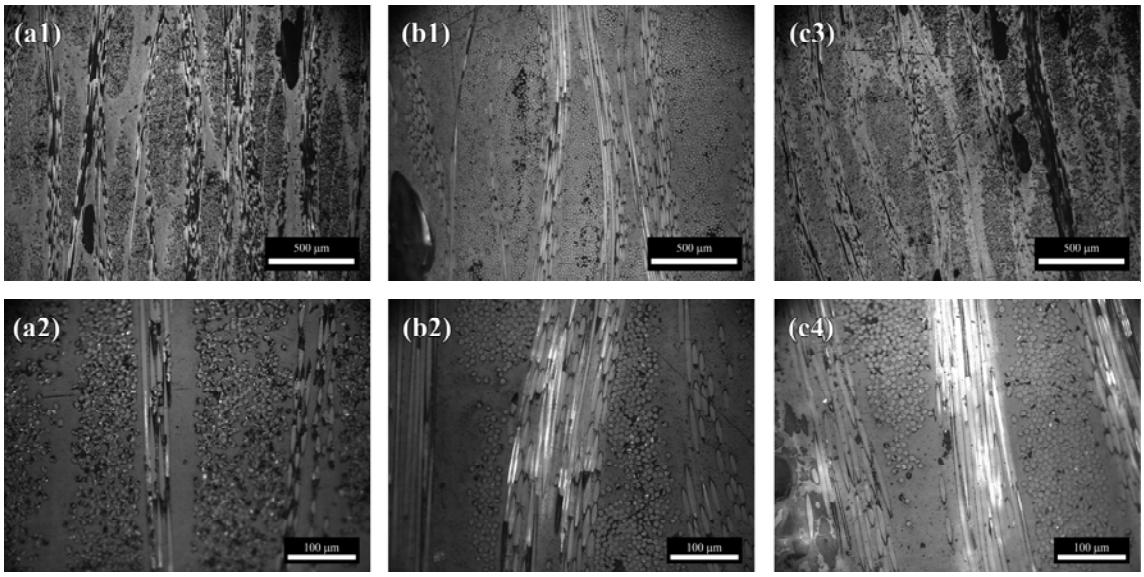

Figure 5: Optical microscopy images of consolidated GF-PA6/Al_2O_3 composite made by soaking the textiles in suspension baths containing (a) 0 g/L, (b) 24 g/L, (c) 78 g/L of Al_2O_3 particles at magnifications of (1) 5 times and (2) 20 times.

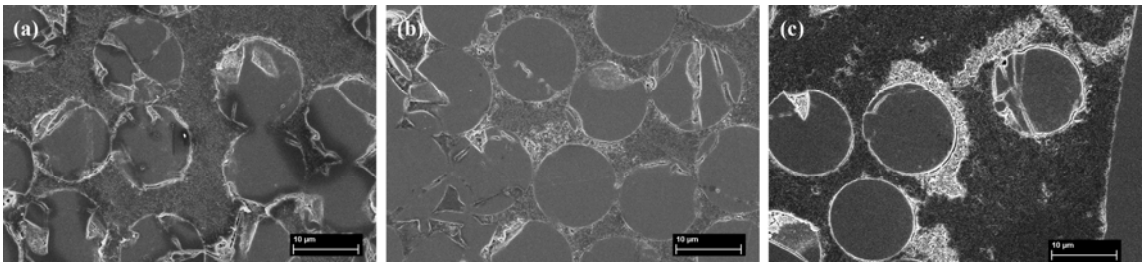

Figure 6: Scanning electron microscopy images showing cross sections with (a) no particles, and after processing in (b) 13 g/L and (c) 78 g/L Al_2O_3 suspensions. Particle agglomerations appear as bright areas typically surrounding the fibres.

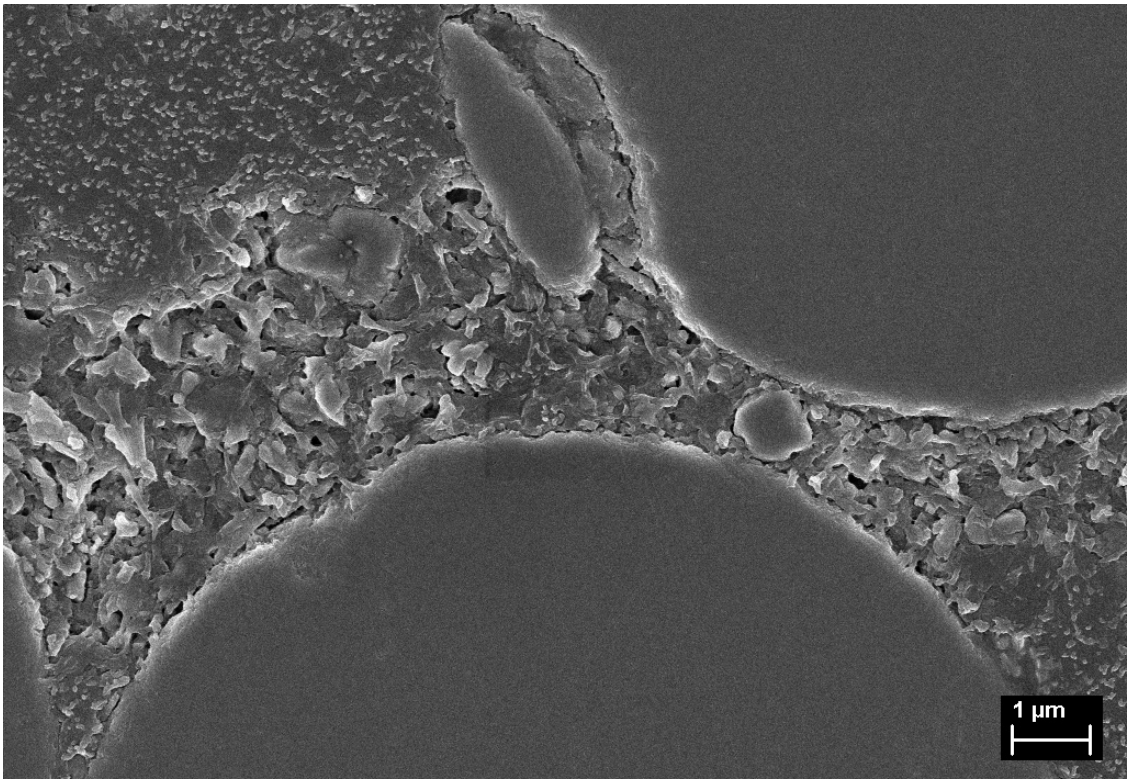

Figure 7: High magnification scanning electron microscope image showing particle-rich and particle-poor regions surrounding a fibre. Particle-poor regions such as the one seen in the upper left corner appear smoother than regions that are particle-rich such as the central area immediately adjacent to the fibre.

3.2 Effects of Al_2O_3 particles in PA6

In the PA6 polymer, the presence of low concentrations (1%) of Al_2O_3 nanoparticles was observed to increase the elastic modulus initially, followed by a sharp decrease at concentrations of 2% vol, with a gradual increase thereafter as shown in Figure 8. The increase in stiffness could be explained by the increasing presence of the higher modulus Al_2O_3 material, while the decrease in stiffness may be attributed in literature to depression of the glass transition temperature (as reported for poly(methyl methacrylate)) due to mechanical interactions between the nanoparticles and the polymer chains.[20] Further investigations would however be needed to confirm this effect for the PA6/Al_2O_3 material system.

Crack opening experiments on SECP specimens (as shown in Figure 1) of PA6 containing varying concentrations of Al_2O_3 particles show that with increasing hard particle content more force was needed to initialize crack growth. However, strain-to-break was reduced significantly by the addition of the particles. The graph in Figure 7 (left) shows representative curves measured from the extruded PA6/Al_2O_3 materials with varying concentrations of Al_2O_3 which were used to derive the J-integral curves shown on the right. The critical strain energy release rates J_{Ic} which mark the onset of crack opening were taken from the point on the J-integral curves where the derivative of the curves ceased to be linear. The results of the J_{Ic} analysis show that fracture toughness is increased by the hard nanoparticles and are plotted in Figure 8.

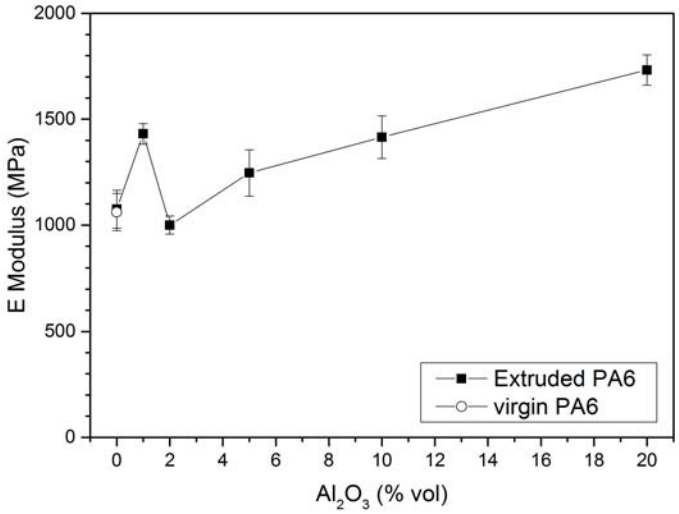

Figure 8: Elastic modulus of Al_2O_3 nanoparticle filled PA6 as a function of filler content

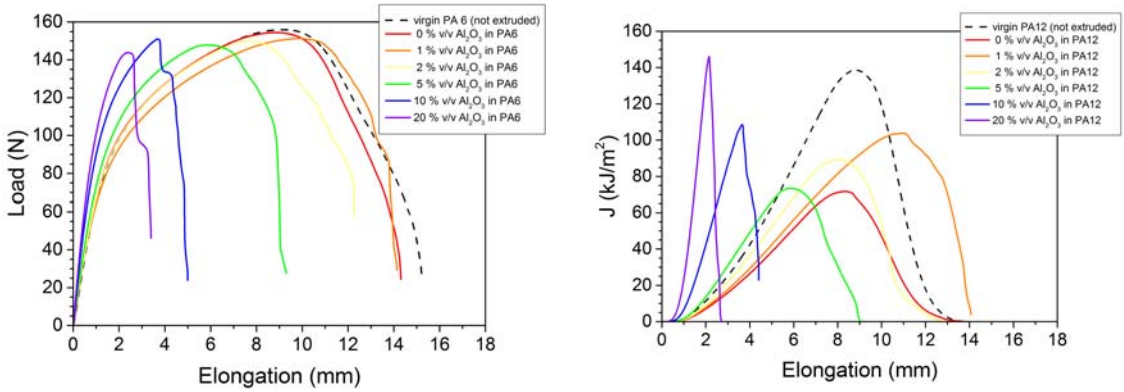

Figure 9: (left) Representative load-elongation curves measured from SECP specimens under uniform tension and (right) the calculated J-integral curves as a function of elongation corresponding to different particle loadings.

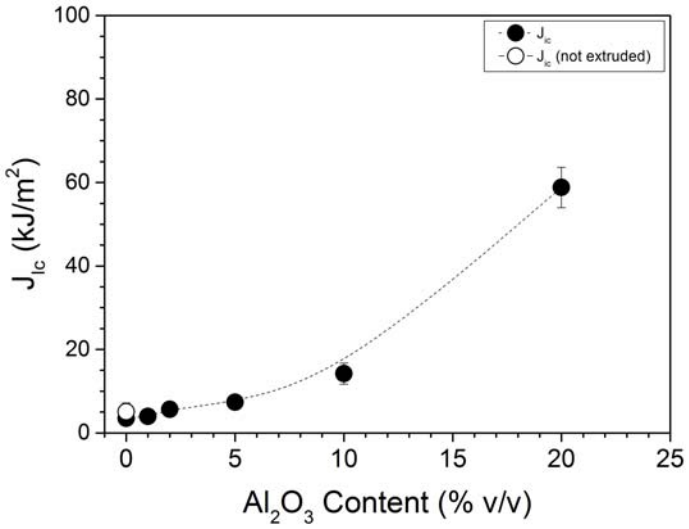

Figure 10: J_{Ic} values of the PA6/Al_2O_3 composites.

3.3 Effects of Al_2O_3 particles in GF-PA6 composites

Premature failure of the specimen by cracking in the through thickness direction and/or by delamination and bending of one of the two cantilever beams, as shown in Figure 11, meant that the interlaminar fracture tests performed on the DCB specimens which contained varying amounts of Al_2O_3 filler did not lead to meaningful results. Examples of these types of failure was observed in members of all the types of material tested; very few samples exhibited instances of stable crack propagation. Transverse yarn debonding, and not delamination through the matrix rich zone, is the likely the preferred mechanism by which these specimens failed. This is in agreement with reports that cracks grow in the regions close to the weft yarn, avoiding the resin-rich payer between the plies needed for delamination failure.[17]

Figure 12 presents sample curves taken from all the different materials tested. Instances of crack propagation was observed in some of the samples made with no suspension bath and those soaked in a suspension containing 24 g/L Al_2O_3. These curves can be distinguished by the relatively flat force-travel relationship shown by the black and orange lines. The fracture surface of the specimens that exhibited limited stable crack propagation were imaged under the SEM to confirm whether or not particles were present on the crack plane. As expected, Figure 13a shows no particles were present at on the crack plane of the sample not treated with the suspension bath, and Figure 13b shows that particles in the form of large agglomerates were abundant on the crack plane in the samples treated in 24 g/L Al_2O_3 suspensions. Higher resolution images, such as the one given in Figure 14 of a smaller particle agglomeration, show evidence of shear band formation in the matrix immediately surrounding an embedded particles. This indicates that the capability of these particles to toughen the fibre-reinforced composite is promising. However, no obvious correlations between the parameters and the force-travel data of the DCB specimens were observed and no further analysis was done on these datasets to determine G_{Ic} values.

Improved sample fabrication methods and experimental design, as well as further investigation will be required to determine whether particles dispersed in the unconsolidated commingled yarns have any effect on the interlaminar fracture strength of fibre reinforced thermoplastic composites.

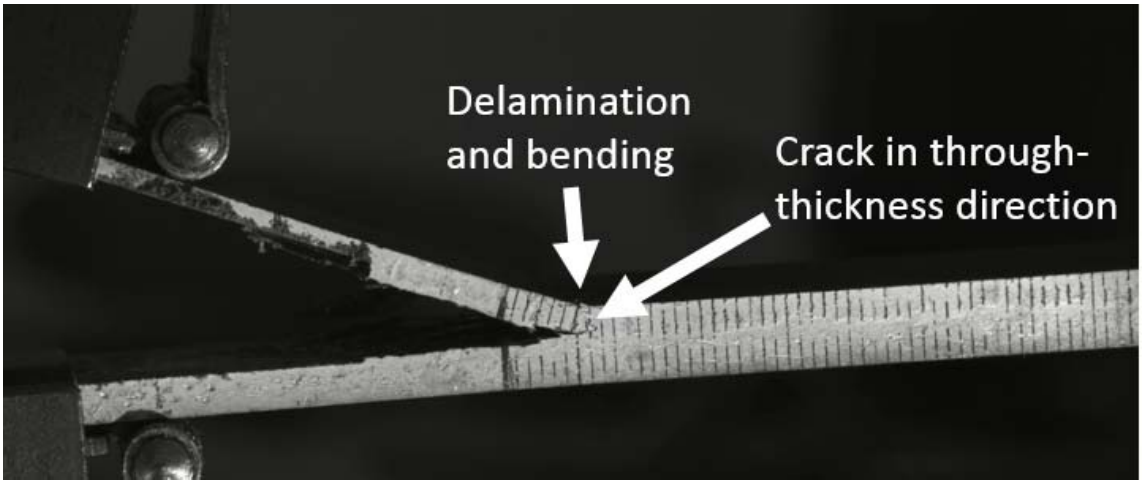

Figure 11: Photograph of double cantilever beam sample undergoing premature failure due to cracking in the through thickness direction and buckling of one of the cantilever beams. Cracks did not propagate through the length of the sample as intended.

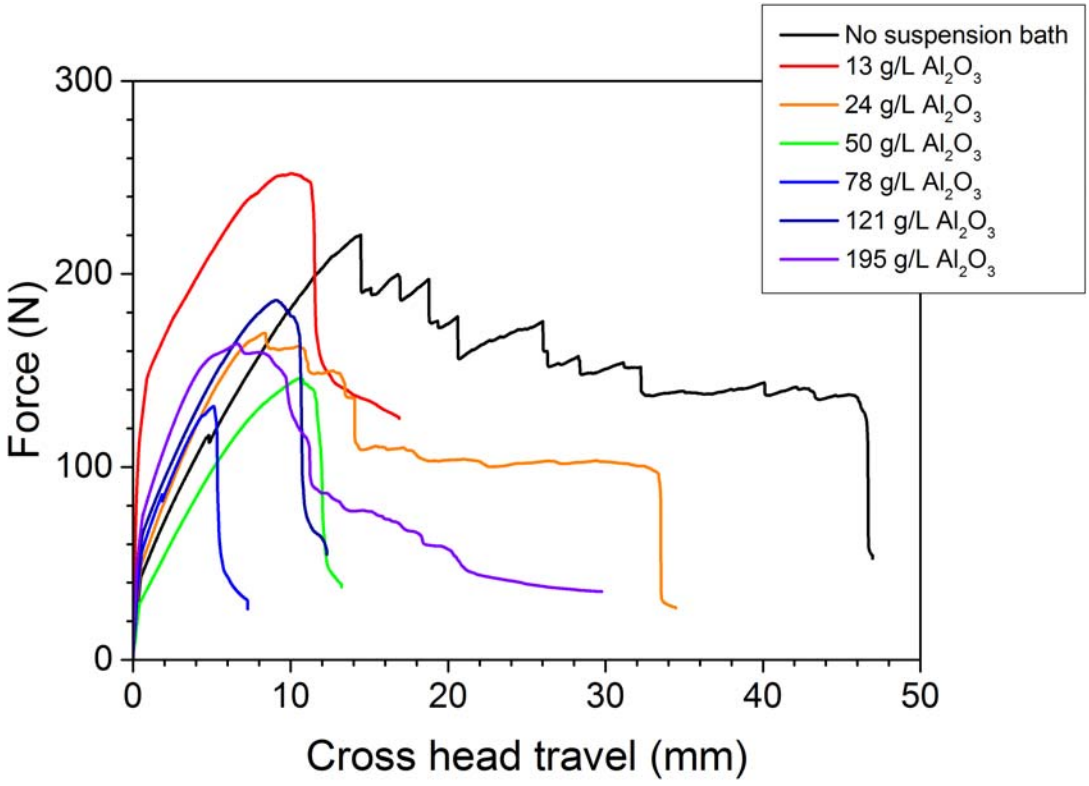

Figure 12: Sample force-travel curves taken from the DCB tests. The black and orange lines represent limited crack propagation. The rest of the lines indicate the samples failed prematurely.

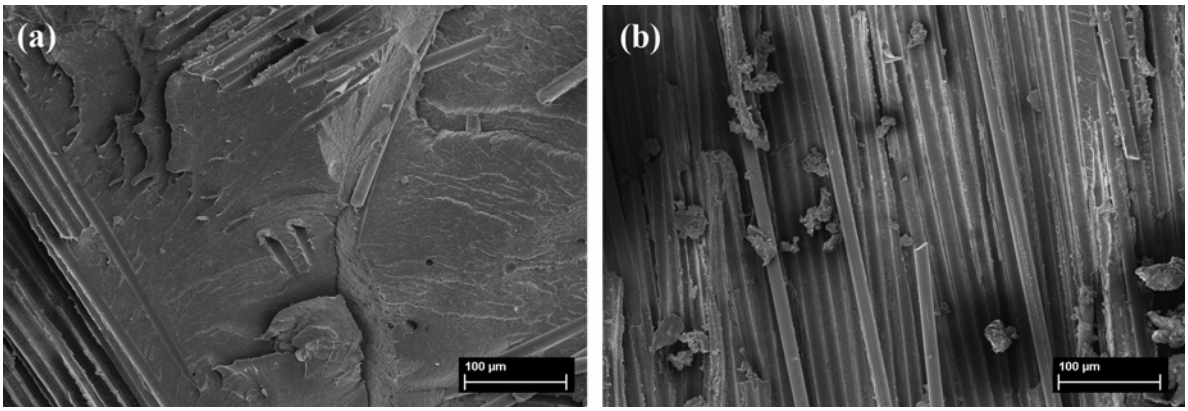

Figure 13: Scanning electron microscopy images of the fracture surface of samples treated with (a) no suspension bath, and (b) 24 g/L Al_2O_3. Particles at the surface show the presence of some particles at the fracture surface.

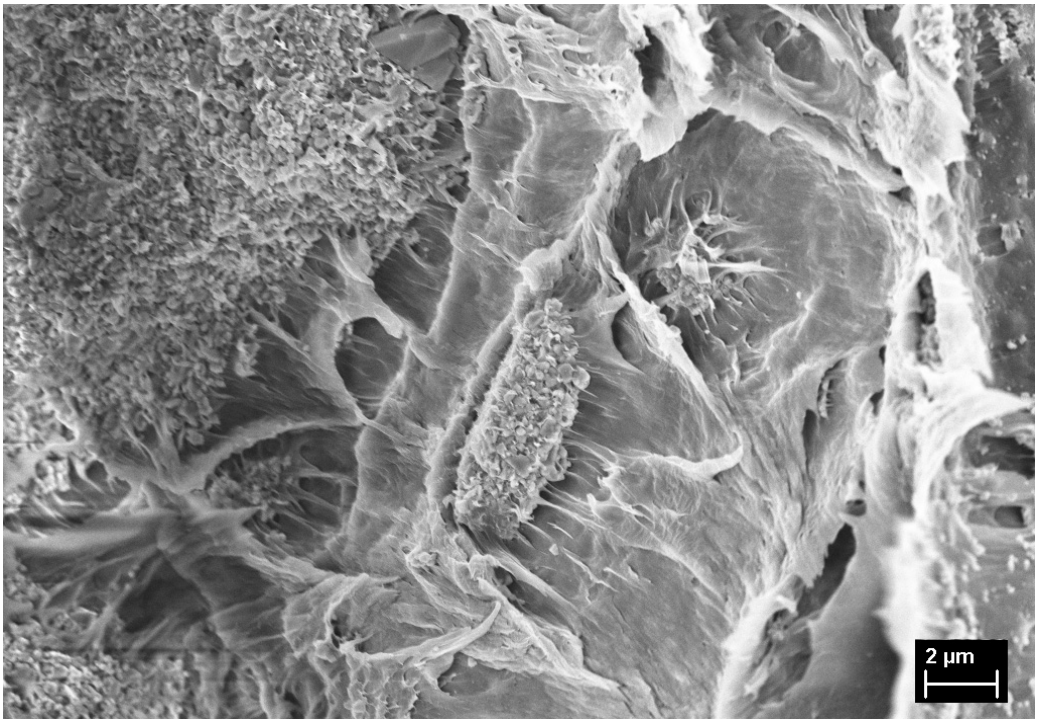

Figure 14: High resolution scanning electron microscopy image of a particle at the fracture surface. Shear bands in the polymer surrounding the particle agglomerate suggest interaction between the particle agglomerate and the crack front.

4 CONCLUSIONS

We have presented a simple method of incorporating hard ceramic fillers into fibre-reinforced thermoplastic composites which disperses the particles relatively evenly inside the commingled yarn fabrics. While the presence of the particles has been shown to increase the E modulus and fracture critical strain energy release rate J_{Ic} of the polymer, we have been unable to experimentally prove that these properties are transferred to the fibre-reinforced composite. The microscopy studies here suggest that the proposed method for creating particle-toughened thermoplastic composites is promising. New experimental designs and further investigations are needed to better measure the effect of the dispersed nanoparticles on the interlaminar fracture toughness G_{Ic} of thermoplastic composites.

ACKNOWLEDGEMENTS

Funding for this work was provided by the Commission for Technology and Innovation (CTI) through the Swiss Competence Center for Energy Research (SCCER) Efficient Technologies and Systems for Mobility. The digital image correlation system was acquired through the SNF R'Equip grant no. 206021_150729. The authors thank Dr. Elena Tervoort for the zeta potential measurements, the Complex Materials group at ETH Zurich for use of their SEM, the Soft Materials group at ETH Zurich for use of their twin screw extruder. The authors also thank Davi Melo Montenegro, Dr. Giulio Molinari, Hanspeter Eigenmann, and Dr. Kirill Feldman for their technical expertise and insightful scientific discussions.

REFERENCES

[1] J. Lee, and A.F. Yee, Inorganic particle toughening I: micro-mechanical deformations in the fracture of glass bead filled epoxies, *Polymer*, **42** (2), 2001, 577-588. (https://doi.org/10.1016/S0032-3861(00)00397-9)

[2] J. Lee, and A.F. Yee, Inorganic particle toughening II: toughening mechanisms of glass bead filled epoxies, *Polymer*, **42** (2), 2001, 589-597. (https://doi.org/10.1016/S0032-3861(00)00398-0).
[3] D.A. Norman, and R.E. Robertson, Rigid-particle toughening of glassy polymers, *Polymer*, **44** (8), 2003, 2351-2362 (https://doi.org/10.1016/S0022-5096(99)00096-4).
[4] M.W.L. Wilbrink, A.S. Argon, R.E. Cohen, and M. Weinberg, Toughenability of Nylon-6 with $CaCO_3$ filler particles: new findings and general principles, *Polymer*, **42**, 2001, 10155-10180 (https://doi.org/10.1016/S0032-3861(01)00548-1).
[5] P.A. Tzika, M.C. Boyce, and D.M. Parks, Micromechanics of deformation in particle-toughened polyamides, *Journal of the Mechanics and Physics of Solids*, **48** (9), 2000, 1893-1929. (https://doi.org/10.1016/S0022-5096(99)00096-4).
[6] B. Geisler, and F.N. Kelley, Rubbery and rigid particle toughening of epoxy resins, *Journal of Applied Polymer Science*, **54** (2), 1994, 177-189 (doi: 10.1002/app.1994.070540204).
[7] J. Lee, and A.F. Yee, Role of inherent matrix toughness on fracture of glass bead filed epoxies, *Polymer*, **41** (23), 2000, 8375-8385 (https://doi.org/10.1016/S0032-3861(00)00186-5).
[8] D.J. Bull, A.E. Scott, S.M. Spearing, and I. Sinclair, The influence of toughening-particles in CFRPs on low velocity impact damage resistance performance, *Composites Part A: Applied Science and Manufacturing*, **58**, 2014, 47-55 (https://doi.org/10.1016/j.compositesa.2013.11.014).
[9] D.J. Bull, S.M. Spearing, and I. Sinclair, Investigation of the response to low velocity impact and quasi-static indentation loading of particle-toughened carbon-fibre composite materials, *Composites Part A: Applied Science and Manufacturing*, **74**, 38-46 (https://doi.org/10.1016/j.compositesa.2015.03.016).
[10] B.M. Louis, F. Klunker, and P.A. Ermanni, Evalution of nanoalumina and nanosilica particle toughened high glass-transition temperature epoxy for liquid composite molding processes, *Journal of Composite Materials*, **50** (11), 2016, 1533-1545 (https://doi.org/10.1177/0021998315594680).
[11] U.T. Gonzenbach, A.R. Studart, E. Tervoort, and L.J. Gauckler, Stabilization of Foams with Inorganic Colloidal Particles, *Langmuir*, **22** (26), 2006, 10983-10988, (doi: 10.1021/la061825a).
[12] U.T. Gonzenbach, A.R. Studart, E. Tervoort, and L.J. Gauckler, Macroporous ceramics from particle-stabilized wet foams, *Journal of the American Ceramic Society*, **90** (1), 2007, 16-22, (doi: 10.1111/j.1551-2916.2006.01328.x).
[13] J.C.H. Wong, E. Tervoort, S. Busato, L.J. Gauckler, and P. Ermanni, Controlling phase distributions in macroporous composite materials through particle-stablized foams, *Langmuir*, **27** (7), 2011, 3254-3260, (doi: 10.1021/la200224k).
[14] J.C.H. Wong, E. Tervoort, S. Busato, P. Ermanni, and L.J. Gauckler, Engineering macroporous composite materials using competitive adsorption in particle-stabilized foams, *Journal of Colloid and Interface Science*, **383** (1), 2012, 1-12, (https://doi.org/10.1016/j.jcis.2012.05.049) .
[15] V. Kumar, M.D. German, and C.F. Shih, An engineering approach for elastic-plastic fracture analysis, (NP-1931 research project 1237-1). Palo Alto, CA: Electric Power Research Institute, 1981.
[16] Standard test method for mode I interlaminar fracture toughness of unidirectional fiber-reinforced polymer matrix composites, *ASTM International*, D5528-13.
[17] N. Alif, L.A. Carlsson, J.W. Gillespie, Mode I, mode II, and mixed mode interlaminar fracture of woven fabric carbon/epoxy, *Composite Materials: Testing and Design*, **13**, ASTM STP 1242, S.J. Hooper, Ed. American Society for Testing and Materials, 1997, 82-106.
[18] F. Brandt, New load introduction concept for improved and simplified delamination beam testing, *Experimental Techniques*, **22** (1), 1998, pp. 17-20. (doi: 0.1111/j.1747-1567.1998.tb00582.x)
[19] J. Renart, N. Blanco, E. Pajares, J. Costa, S. Lazcano, and G. Santacruz, Side clamped beam (SCB) hinge system for delamination tests in beam-type composite specimens, *Composites Science and Technology*, **71**, 2011, pp. 1023-1029. (doi: 10.1016/j.compscitech.2010.10.005)
[20] B.J. Ash, D.F. Rogers, C.J. Wiegand, L.S. Schadler, R.W. Siegel, B.C. Benicewicz, and T. Apple, Mechanical properties of Al_2O_3/polymethylmethacrylate nanocomposites, *Polymer Composites*, **23** (6), 2002, pp. 1014-1025 (doi: 0.1002/pc.10497).